Title

Effect of threading dislocation density on Ni/n-GaN Schottky diode I-V characteristics

Journal

Journal of Applied Physics, 100(2)

ISSN

0021-8979

Authors

Arehart, A R
Moran, B
Speck, J S
et al.

Publication Date

2006-07-01

Peer reviewed

Effect of threading dislocation density on Ni/*n*-GaN Schottky diode *I-V* characteristics

A. R. Arehart
Department of Electrical and Computer Engineering, The Ohio State University, Columbus, Ohio 43210

B. Moran, J. S. Speck, U. K. Mishra, and S. P. DenBaars
Materials and Electrical and Computer Engineering Departments, University of California, Santa Barbara, California 93106

S. A. Ringel[a)]
Department of Electrical and Computer Engineering, The Ohio State University, Columbus, Ohio 43210

(Received 12 January 2006; accepted 14 May 2006; published online 21 July 2006)

The impact of threading dislocation density on Ni/*n*-GaN Schottky barrier diode characteristics is investigated using forward biased current-voltage-temperature (*I-V-T*) and internal photoemission (IPE) measurements. Nominally, identical metal-organic chemical vapor deposition grown GaN layers were grown on two types of GaN templates on sapphire substrates to controllably vary threading dislocation density (TDD) from 3×10^{7} to 7×10^{8} cm^{-2}. *I-V-T* measurements revealed thermionic emission to be the dominant transport mechanism with ideality factors near 1.01 at room temperature for both sample types. The Schottky barrier heights showed a similar invariance with TDD, with measured values of 1.12–1.13 eV obtained from fitting the *I-V-T* results to a thermionic emission-diffusion model. The *I-V-T* results were verified by IPE measurements made on the same diodes, confirming that the Ni/*n*-GaN barrier heights do not show a measurable TDD dependence for the TDD range measured here. In apparent contrast to this result is that the measured forward bias *I-V* characteristics indicate a shift in the observed forward bias turn-on voltage such that at the higher TDD value investigated here, a larger turn-on voltage (lower current) is observed. This difference is attributed to localized current blocking by high potential barrier regions surrounding threading dislocations that intersect the Ni/GaN interface. A simple model is presented that reconciles both the observed voltage shift and variations in the extracted Richardson constant as a function of threading dislocation density. With this model, an average local barrier surrounding dislocation of ~0.2 V is obtained, which diverts current flow across the forward biased Schottky interface to nondislocated regions. © *2006 American Institute of Physics*.
[DOI: 10.1063/1.2219985]

I. INTRODUCTION

Detailed understanding and optimization of GaN and AlGaN Schottky barrier properties are critical for III-nitride device technologies such as high power high electron mobility transistors (HEMTs) and solar-blind detectors.[1–3] Maximizing the Schottky barrier height, minimizing reverse leakage current, and minimizing their variation over large area are all key to advancing the performance of these devices and to enhance manufacturability. Considerable efforts continue to be made to explore factors that influence GaN Schottky diodes, which historically had been motivated by basic studies of III-N materials and metal/GaN interfaces.[4–8] Throughout the literature, studies have revealed various dependencies of the Schottky barrier height on the forward bias ideality factor,[4] choice of Schottky metal,[5,6] influence of surface damage,[7] and material quality.[8] Due to the importance of these parameters in ultimate device applications, quantitative determination of their values and factors that affect their accuracy within the usual current-voltage models that are applied to this problem need to be understood. This paper describes the impact of controlled threading dislocation density (TDD) variation on the barrier height of Ni/*n*-GaN Schottky diodes fabricated on metal-organic chemical vapor deposition (MOCVD) grown *n*-type GaN, and explores fundamental issues pertaining to the accuracy of barrier height determination using *I-V* analysis for GaN with non-negligible dislocation density. It is shown that for the samples studied here the Schottky barrier height (SBH) is independent of TDD over a range of 3×10^{7}–7×10^{8} cm^{-2}, and this is verified using independent internal photoemission (IPE) and current-voltage-temperature (*I-V-T*) measurements. In addition, the lower TDD sample shows near ideal Schottky behavior that follows a simple Richardson model. However, the Schottky diode with higher TDD displays significant deviations in the detailed *I-V* characteristics that are explained by the influence of an inhomogeneous Ni/GaN interface attributed to the non-negligible presence of threading dislocations. This is shown to yield anomalously small Richardson constant values and erroneous extraction of Schottky barrier height using *I-V* analysis, if not properly accounted.

[a)]Electronic mail: ringel.5@osu.edu

II. EXPERIMENTAL DETAILS

A. Sample preparation

Nominally identical, unintentionally doped (uid) *n*-type GaN layers were grown by MOCVD on two types of GaN templates on sapphire designed to provide a wide variation in TDD for these studies. One template consisted of a ~3 μm thick atmospheric pressure MOCVD grown GaN film with the last ~2 μm Si doped to $\sim 3\times 10^{18}$ cm^{-3} deposited on a *c*-plane sapphire substrate. The second template was a commercial *n*-type Lumilog 2S-LEO (two step lateral epitaxially overgrown) substrate. The uid *n*-GaN layers were grown to a thickness of 0.8 μm under atmospheric pressure at 1040 °C on each substrate. *C-V* measurements confirmed similar background electron concentration values in each case of $\sim 1\times 10^{16}$ cm^{-3}. Subsequent electron-beam-induced current (EBIC) measurements of the uid GaN layers revealed an average TDD value of 7×10^{8} cm^{-2} for the former (higher TDD sample) and 3×10^{7} cm^{-2} for the latter (lower TDD sample). This provided a factor of ~20 difference in TDD between the two sample types—to support the goals of this study.

The samples were processed into square mesa-etch structures and had areas varying from 0.04 to 0.23 mm^2. The top contact, required to be semitransparent to transmit light for the IPE experiment, was 80 Å thick Ni and also served as the Schottky contact. To define the mesa and etch down to the heavily doped lateral conduction layer for later back contact deposition, reactive ion etching (RIE) was performed. The RIE process was done at 40 W using 20 SCCM (SCCM denotes standard cubic centimeter per minute at STP) Cl_2, 5 SCCM Ar, a pressure of 5 mTorr, and a 145 V dc bias. The back contact was a Ti/Al/Ni/Au Ohmic contact deposited on the heavily doped MOCVD template layer. Prior to diode fabrication, the samples were cleaned with an acetone/methanol rinse. To define the Schottky metal contact area, one photolithography process was needed. After developing the photoresist, the samples were put in an O_2 barrel asher for 2 min, dipped in HCl:DI (de-ionized) water [1:1] for 30 s, and rinsed in DI water before e-beam evaporating the 80 Å thick Ni layer. No annealing was used for these samples. Further details of the test structure and fabrication can be found elsewhere.[9]

B. Current-voltage-temperature (*I-V-T*) measurements and analysis

I-V-T measurements were performed in the dark using a cryostat capable of temperatures from 85 to 400 K. *I-V* characteristics were obtained with an HP 4145B after the temperature stabilized in increments of 10 K. The ideality factor and saturation current parameters were extracted from the linear regime of the forward bias *I-V* characteristic, which for these diodes spanned between four and eight decades of linearity. The standard diode equation used to extract the *I-V* parameters is

$$\ln(I) = \frac{qV}{nkT} + \ln(I_s) \quad \text{for } qV > 3kT, \tag{1}$$

where q is the electron charge, k is Boltzmann's constant, and T is the temperature. From Eq. (1), we can extract the ideality factor n and the saturation current I_s, which is expressed as[10]

$$I_s = A_e A^* T^2 \exp\left(\frac{-q\Phi_{b0}}{kT}\right). \tag{2}$$

The device area A_e can also be used to calculate the current density J by dividing I by the device area. After rearranging, the Richardson constant A^* and zero-bias barrier height Φ_{b0} can be obtained from

$$\ln\left(\frac{I_s}{A_e T^2}\right) = \ln A^* - q\Phi_{b0}\frac{1}{kT}. \tag{3}$$

Plotting $1/kT$ vs $\ln(I_s/A_eT^2)$ is referred to as a Richardson plot, where the slope is the barrier height and the y intercept is $\ln(A^*)$. The theoretical Richardson constant with units of A K^{-2} cm^{-2} is given by[10]

$$A^* = \frac{4\pi q m^* k^2}{h^3} = 120\frac{m^*}{m_0}, \tag{4}$$

where h is Planck's constant, m^* is the majority carrier effective mass, and m_0 is the free electron mass. By assuming a value for the electron effective mass in GaN of $0.222m_0$,[11] the theoretical Richardson constant for *n*-type GaN is found to be 26.64 A K^{-2} cm^{-2}.

C. Photoemission experiments

IPE experiments were performed to provide an independent measure of the Schottky barrier height that is not dependent upon the various parameters necessary for *I-V-T* modeling and analysis so that *I-V-T* results could be verified. The IPE measurements were conducted by illuminating the sample through the semitransparent Schottky contacts with monochromatic light and measuring the resulting photocurrent at zero voltage bias. If the photon is absorbed in the metal, an electron is excited above the Fermi level. If the electron has energy greater than or equal to the Schottky barrier height and diffuses towards the metal/semiconductor interface, the electron can enter the semiconductor and be swept away in the Schottky barrier's electric field thus creating a photocurrent. For photon energies, $h\nu$, several kT greater than the Schottky barrier height Φ_b^{IPE}, the photoyield R can be expressed as[10,12]

$$R \sim (h\nu - \phi_b^{\mathrm{IPE}})^2, \tag{5}$$

where R is the number of electrons collected per second divided by the number of photons incident per second. By plotting the photon energy versus the square root of the photoyield, a straight line is achieved and by extrapolating to the x axis, the barrier height can be determined. The measurement was performed in ambient dark with photoexcitation provided by a 1000 W xenon lamp passed through an Oriel Cornerstone 260 monochomator. A Keithley 617 electrometer with shielded cables from the shielded sample holder

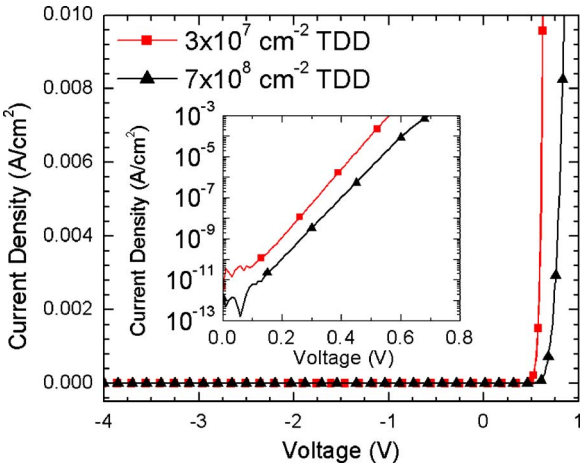

FIG. 1. (Color online) Current density vs applied voltage data for the lower TDD (3×10^7 cm^{-2}) (■) and high TDD (7×10^8 cm^{-2}) (▲). The inset shows the same data in log current density vs applied voltage. The devices show an apparent variation in turn-on voltage.

was used to measure the resulting photocurrent. The photon flux density was measured at the plane of the semiconductor with an Oriel thermopile with a shadow mask of known area. The thermopile has the advantage of having a very flat response over a large range of photon energy. At any given photon energy of approximately 10^{15} photons/s cm^2 were incident on the top of the 80 Å Ni Schottky contact.

III. RESULTS AND DISCUSSION

A. Current-voltage characteristics and Schottky barrier height dependence on TDD

A plot of current density versus voltage is shown in Fig. 1 for the high and low TDD samples. At first glance, it appears that the change in dislocation density causes a change in the forward bias turn-on voltage such that the high TDD sample displays a higher apparent built-in voltage. However, this in fact is not the case, and quantitative measurements (*I-V-T* and IPE) reveal the probable mechanism that explains this observation. Using Eq. (1), the saturation current and ideality factor at each temperature were extracted from the linear regions of the *I-V* curves shown in Fig. 2. Using only the linear region assures negligible influence from series resistance. The low TDD sample had a linear region of approximately seven decades and the high TDD sample had approximately five decades of linearity, indicating that both are of high quality. Additionally, the low TDD diode had an ideality factor of 1.01 at room temperature with only slight temperature dependence, while the high TDD diode had an ideality factor of 1.04. At 150 K, the low TDD sample had an ideality factor of 1.05, whereas the ideality factor of the high TDD sample increased somewhat to 1.38 at 150 K. The negligible temperature dependence of the low TDD sample suggests that thermionic-field emission (TFE) and field emission are negligible and that thermionic emission (TE) is the dominant transport mechanism. However, the slight increase in n for the higher TDD device implies a change in the dominant current transport mechanism. Theo-

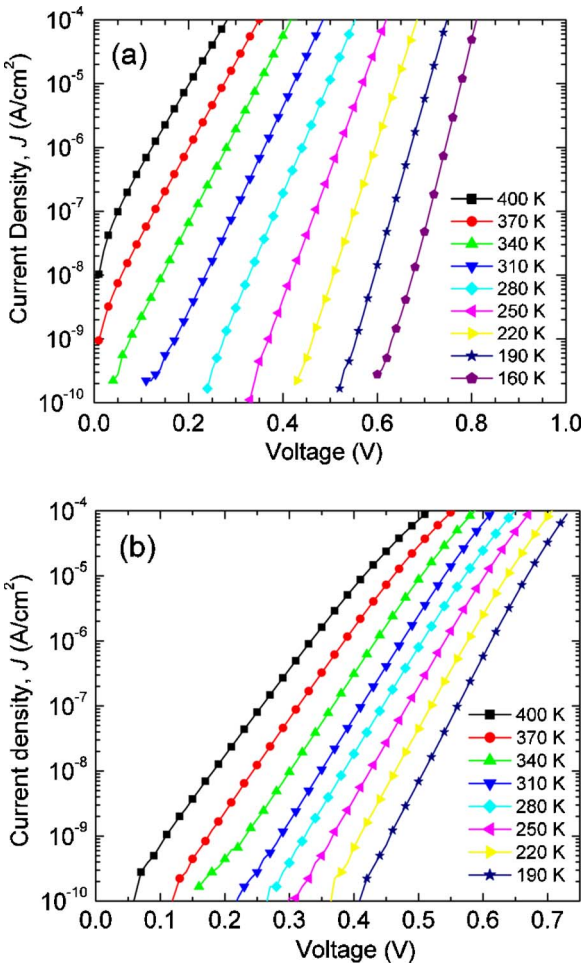

FIG. 2. (Color online) Current density vs applied voltage data at selected measurement temperatures for the lower TDD (3×10^7 cm^{-2}) sample and higher TDD (7×10^8 cm^{-2}) sample in (a) and (b), respectively. Data were taken in 10 K increments.

retically, TFE becomes important when its characteristic energy E_{00} is comparable to kT, where E_{00} is given by[13]

$$E_{00} = \frac{h}{4\pi}\left(\frac{N_D}{m_e^* \varepsilon_s}\right)^{1/2}, \tag{6}$$

where ε_s is the permittivity of GaN and the TFE-dominated ideality factor n_{00} is given by

$$n_{00} = \frac{E_{00}}{kT}\cosh\left(\frac{E_{00}}{kT}\right). \tag{7}$$

By plotting the ideality factor versus temperature and comparing with Eq. (7), E_{00} can be estimated, which was approximately 4 meV for the low TDD sample. The high TDD sample E_{00} energy was somewhat higher, roughly 15 meV. However, TFE transport only becomes comparable to TE transport when kT is comparable to E_{00}, which only occurs for the higher TDD sample and at the lowest measurement temperatures. Thus from this analysis, thermionic emission is dominant for both samples, with TFE playing a minor role for the higher TDD devices, consistent with the near unity ideality factors for both samples over the entire temperature range.

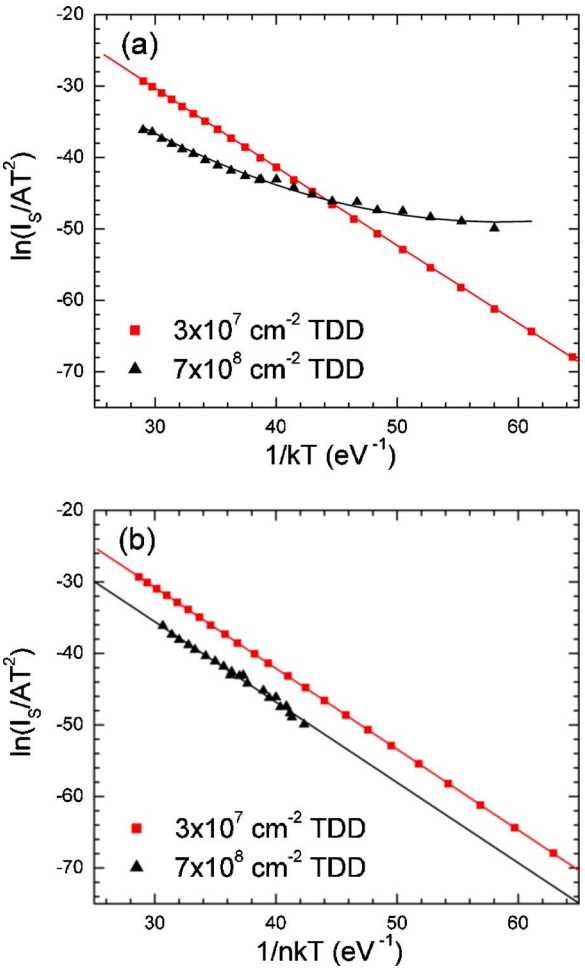

FIG. 3. (Color online) (a) Richardson plot $[\ln(I_s/AT^2)$ vs $1/kT]$ and (b) the same data plotted with the modified Richardson plot $[\ln(I_s/AT^2)$ vs $1/nkT]$ for the lower TDD (■) and higher TDD (▲) samples.

Having established thermionic emission as the dominant transport mechanism for both Schottky devices, we can now determine and compare the Schottky barrier heights using an Arrhenius analysis. Figure 3(a) shows the Richardson plot $[\ln(I_s/AT^2)$ vs $1/kT]$ for the lower TDD device that was obtained by fitting the extracted values of I_s from the *I-V-T* data in Fig. 2(a) to Eq. (3). The excellent linearity allows simple extraction of both the Schottky barrier height and Richardson constant and were found to be 1.13 V and 23 A K^{-2} cm^{-2}, respectively, for the lower TDD devices. The same procedure was followed for the higher TDD sample, but because the Richardson plot deviates from linearity at lower measurement temperatures due to the small increase in ideality factor with reduced temperature as described above, only the higher measurement temperature regime was initially considered for fitting to Eq. (3). This yielded an extracted barrier height of ~1.10 eV near room temperature, similar to the value for the lower TDD samples. To analyze the full temperature dependence, however, the modified Richardson plot $[\ln(I_s/AT^2)$ vs $1/nkT]$ was used, which linearizes the plot with respect to $1/kT$ due to the slight temperature dependence of n. Such nonlinearities have been commonly reported and various mechanisms have been used to explain the need for including n in the Richardson plot,

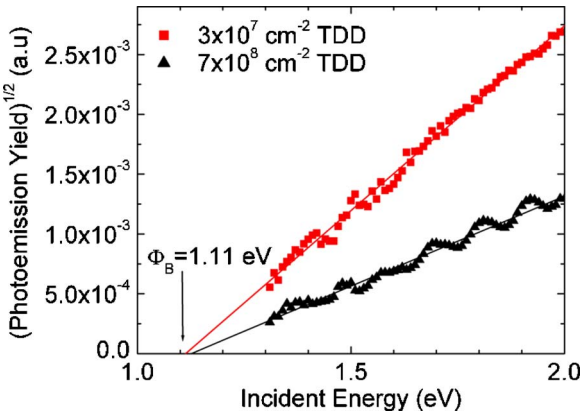

FIG. 4. (Color online) IPE results shown by plotting the square root of photoyield as a function of incident photon energy. The Schottky barrier height, extracted from the x intercept, shows nearly identical SBHs independent of TDD from 3×10^7 to 7×10^8 cm^{-2} for the lower TDD (■) and higher TDD (▲) samples, respectively.

such as image forces, tunneling currents, and spatial distribution of charged defects, none of which are accounted for in Eq. (3).[14,15] Additionally, Werner and Güttler showed that this relationship can be described in terms of barrier height inhomogeneity, a point that will be explored in more depth later.[16] As seen from Fig. 3(b), the modified Richardson plot greatly improves linearity of the data for the higher TDD sample. With this model, a Schottky barrier height of 1.12 eV was found, which closely matches the fit to the higher temperature data using Eq. (3) where simple thermionic emission is dominant for the higher TDD sample, providing validity to this approach. It is particularly remarkable that nearly identical Schottky barrier heights were determined for the lower and higher TDD samples, in apparent contrast to the observed *I-V* behavior shown in Fig. 1.

To provide an independent measure of the barrier heights that is free of model-dependent parameter fitting from *I-V* measurements, we performed IPE measurements on the same diodes. Figure 4 shows the IPE results, from which the barrier height was obtained by graphing the incident light energy versus the square root of the photoyield and extrapolating a line to the x axis according to Eq. (5). At the x axis, the photoyield is zero and the incident light energy equals the Schottky barrier height. The barrier heights, obtained using IPE, were indeed between 1.11 and 1.13 eV for both TDD values, in close agreement with the values obtained from the *I-V-T* measurements and various analysis methods. Table I compiles the Schottky diode parameters determined from both *I-V-T* and IPE analyses. Since IPE does not depend on parameters used to model current transport behavior it provides a simple and independent measurement of the SBH values. Thus, if a variation in SBH between samples is not responsible for the shift in the forward bias turn-on shown in Fig. 1, the question is what else may be responsible. The only apparent difference between the diodes is in the value for the extracted Richardson constant, which as seen in Table I is near ideal for the lower TDD sample [see Eq. (4)] but is substantially reduced for the higher TDD sample. The next section explores the source of this discrepancy in greater detail.

TABLE I. Extracted values for barrier heights from *I-V-T* and IPE measurements and models. Also shown are measured ideality factors and the extracted Richardson constant.

Sample	Threading dislocation density (cm^{-2})	*I-V-T* barrier height Φ_{b0} (V)	IPE barrier height Φ_b^{IPE} (V)	Room temperature ideality factor n	Extracted Richardson constant A^* ($A\,K^{-2}\,cm^{-2}$)	
					Without model	Assuming $r=200$ nm
Lower TDD	3×10^7	1.13	1.11	1.01	23	24
Higher TDD	7×10^8	1.12	1.13	1.04	0.16	24

B. Reconciliation of the Richardson constant and impact of threading dislocations on forward bias *I-V* characteristics

As just described, the apparent inconsistency between the invariant Schottky barrier heights and the shift in the *I-V* forward bias turn on as a function of TDD requires more rigorous analysis. It shows that a review of the literature reveals many reports of large variations in the extracted Richardson constant for *n*-GaN Schottky diodes using simple *I-V* models with reported values ranging from 0.006 to 102 $A\,K^{-2}\,cm^{-2}$.[17–19] This large variation is reported despite the fact that the Richardson constant is a fundamental parameter that depends only on the semiconductor material constants, and thus should not display significant dependencies on Schottky metal, TDD, etc. This calls into question the simple extraction of Richardson constants as is commonly done in *I-V* analysis as described in Sec. III A. To review, extracting the Richardson constant from the Richardson plot in Fig. 3 for the lower TDD reveals a value of 23 $A\,K^{-2}\,cm^{-2}$, in reasonable agreement with the theoretically predicted value of 26.64 $A\,K^{-2}\,cm^{-2}$. However, the same approach applied to the higher TDD sample yields a much lower value of 0.16 $A\,K^{-2}\,cm^{-2}$, highlighting this anomaly (Table I). Note that the small Richardson constant is manifested in a reduction of saturation current at all temperatures for the higher TDD sample. Previous reports have attributed variations in the fitted Richardson constant to enhanced tunneling current, interfacial oxide layers, or lateral Schottky barrier height variation.[17–23] However, since we find that the current of the higher TDD sample is always *lower* than the current of the lower TDD sample at all forward bias voltages, it is unlikely that tunneling is responsible for the deviation, since an additional parallel transport mechanism will only add current in forward bias as would any regions of reduced barrier heights associated with the higher dislocation density. The similarity of the barrier heights and ideality factors for both types of samples supports the assertion that tunneling is negligible and that an interfacial layer is absent.

Since this discussion rules out different fundamental transport mechanisms between the two samples or the presence of parallel transport mechanisms as being responsible for the observed difference in *I-V* characteristics, more investigation is required about how threading dislocations that intersect the Ni/*n*-GaN Schottky interface may impact local current transport. If the dislocations acted as simple shunt or recombination current pathways, the higher TDD sample would show a smaller turn-on voltage than the lower TDD sample, not vice versa. This leads us to suggest that dislocations are instead acting to impede current flow in localized regions, in effect causing a lateral inhomogeneity in which TD-localized regions restrict and divert current flow. This idea is supported by scanning capacitance microscopy studies[24] that showed evidence for significant negative charge buildup in the local vicinity of dislocations intersecting *n*-GaN surfaces causing higher localized Schottky barrier heights with respect to the surrounding material. This effect has also been observed by scanning Kelvin probe microscopy studies that reported an increase in surface potential of as much as 0.3–0.5 V across threading dislocations intersecting *n*-GaN surfaces, with a spatial full width at half maximum (FWHM) of 30–50 nm.[25] Other reports have suggested that dislocations can influence local current transport via other effects such as local oxidation,[26,27] which also would impede local current flow. Additionally, there have been several reports that show dislocations of pure edge or mixed character tend to generate highly localized regions of reduced carrier conduction in GaN grown by molecular beam epitaxy (MBE) on nominally identical MOCVD GaN templates as used in this current study and these TDs are predominantly of pure edge or mixed character.[28–30] Clearly there is ample microscopic evidence to support our macroscopic observations over the range of dislocation densities we are concerned with here. These apparent correlations aside since a direct study of such correlations are beyond the scope of this paper, we conclude that erroneous assignment of forward bias *I-V* parameters will result if the localized impact of dislocations on the lateral uniformity of current transport is not considered.

In an attempt to account for this effect so that Richardson constant values can be reconciled using *I-V* analysis, we construct a simple equivalent circuit model for an *n*-GaN Schottky diode. The model consists of two Schottky diodes in parallel such that one represents the total interface area where there is negligible impact of crossing dislocations and another higher barrier region that represents the total interface area where dislocations impact the local barrier height. Thus, the total diode current is simply the sum of the currents from the two SBH regions. If we now assume, for simplicity, that each dislocation is surrounded by a local, radially symmetric region of higher barrier, the fraction of the entire interface area A_e, attributed to the higher barrier regions A_d, can be expressed as

$$A_d = [\mathrm{TDD}]A_e \pi r^2. \tag{8}$$

Here, TDD is the threading dislocation density intersecting the Ni/GaN interface and r is the effective radius of a cylindrical area surrounding each dislocation. The effective area A_n of the intimate Ni/GaN contact that does not include the localized effects of the dislocations is thus

$$A_n = A_e(1 - [\mathrm{TDD}]\pi r^2). \tag{9}$$

The total saturation current can now be represented as

$$I_s = A^* T\left[A_n \exp\left(\frac{-q\Phi_{b0}}{kT}\right) + A_d \exp\left(\frac{-q\Phi_{bd}}{kT}\right)\right], \tag{10}$$

where the lower and higher barrier heights are Φ_{b0} and Φ_{bd}, respectively. This expression is difficult to solve analytically, but since the current flow depends exponentially on the SBH and prior work has shown local barriers can be ~0.3–0.5 eV higher than surrounding barriers in the field,[25] even a small increase in barrier height will result in a negligible current contribution from the higher SBH regions. Thus, we choose to ignore contributions from the second term in this simple model (the validity of this assumption is considered later). The resulting expression combining Eqs. (9) and (10) is

$$I_s = A_e(1 - \pi r^2[\mathrm{TDD}])A^* T^2 \exp\left(\frac{-q\Phi_{b0}}{kT}\right). \tag{11}$$

The theoretical Richardson constant in Eq. (4) has several assumptions and neglects scattering events and thus only provides a reasonable estimate of the true Richardson constant. Nevertheless, the Richardson constant is a fundamental parameter that cannot really vary from sample to sample, so it is reasonable to assume that the Richardson constant of the lower and higher TDD samples is the same. With this in mind, Eq. (11) can be rearranged to

$$A^* = \frac{I_s}{T^2 A_e(1 - \pi r^2[\mathrm{TDD}])} \exp\left(\frac{q\Phi_{b0}}{kT}\right). \tag{12}$$

This allows Eq. (12) to be developed for both the higher and lower TDD samples leaving only A^* and r unknown. Inserting known values of TDD, saturation current, and barrier height for each sample, the expression for both samples can be simply equated since A^* is constant for both samples and is eliminated according to Eq. (13) from which r can be determined, viz.,

$$\frac{I_{s1}}{1 - \pi r^2[\mathrm{TDD}_1]} \exp\left(\frac{q\Phi_{b01}}{kT}\right) = \frac{I_{s2}}{1 - \pi r^2[\mathrm{TDD}_2]} \exp\left(\frac{q\Phi_{b02}}{kT}\right), \tag{13}$$

where T is 300 K, $[\mathrm{TDD}_1]$ is 3×10^7 cm^{-2} for the lower TDD sample, $[\mathrm{TDD}_2]$ is then 7×10^8 cm^{-2}, Φ_{b01} and Φ_{b02} are the respective barrier heights from the *I-V-T* analysis, and I_{s1} and I_{s2} are the room temperature saturation currents for the lower and higher TDD samples, respectively. Following this approach, r can be solved for explicitly and an approximate value of 190 nm is obtained. If this value is reasonable then reinserting it into Eq. (12) should yield a reasonable value for A^*, which is 24 A K^{-2} cm^{-2}—very near the theoretically predicted value of 26.64 A K^{-2} cm^{-2}, for both the higher and lower TDD samples. Moreover, earlier studies using scanning capacitance measurements performed on MOCVD grown *n*-GaN samples reported local raised barrier height regions of similar length scale to the radius determined in this study.[24] Finally, it is important to note, as shown in Fig. 5(b), that this correction has no effect on the extracted SBHs and so remains consistent with the SBHs extracted from the *I-V-T* and IPE measurements.

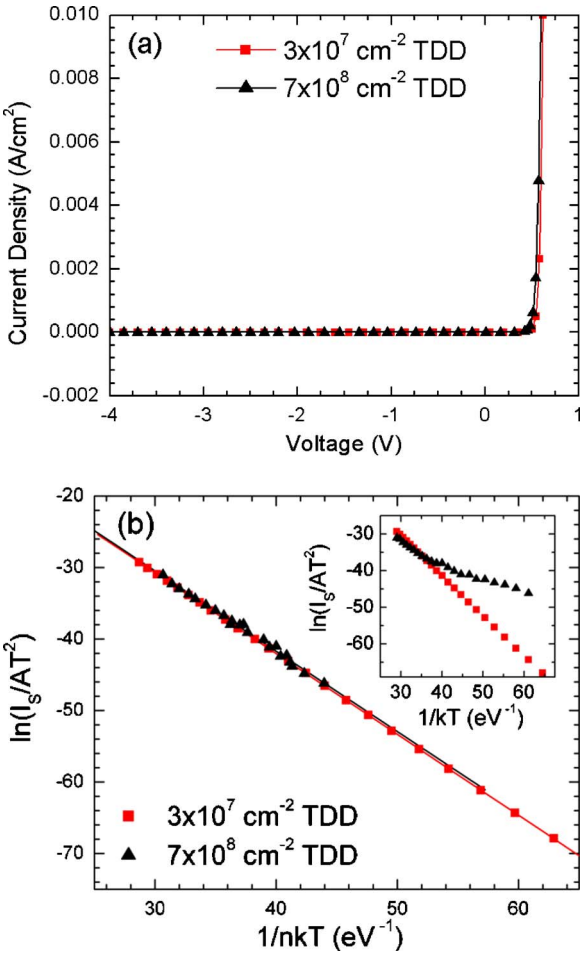

FIG. 5. (Color online) (a) Current density vs applied voltage data for the lower TDD (3×10^7 cm^{-2}) (■) and high TDD (7×10^8 cm^{-2}) (▲) samples excluding the higher SBH regions by correcting the active device area using Eq. (9). The curves now have very similar turn-on voltages consistent with IPE and *I-V-T* results. (b) Modified Richardson plot [$\ln(I_s/AT^2)$ vs $1/nkT$] for the lower TDD (■) and higher TDD (▲) samples also correcting for the active device area. The inset shows the same data plotted with the normal Richardson plot [$\ln(I_s/AT^2)$ vs $1/kT$].

Using this simple approach, we can revisit and reconcile the turn-on voltage issue of Fig. 1. We apply this model to the measured current density versus voltage (*J-V*) characteristics of Fig. 1 by scaling the device areas to match only that of the ideal Schottky regions that exclude the localized high barrier areas for both the higher and lower TDD devices, by which we obtain the recalculated *J-V* data shown in Fig. 5(a). A very good agreement is now observed, strongly suggesting that current blocking in the vicinity of dislocation crossings at the Schottky interface causes the observed difference in turn-on voltage and current blocking. Moreover, the near uniform reduction in the saturation current

density values for the higher TDD sample as seen in the Richardson plot of Fig. 3, for which total device areas rather than corrected areas were used, is no longer present, as seen in Fig. 5(b).

While it is important to note that we cannot ascribe this effect to a specific physical source as our analysis only measures its impact on current flow, we can, by assuming the effect is due to localized space charge, calculate the local barrier heights and spatial extent of these TD-associated regions to provide additional plausibility of this simple model. By assuming a symmetrical, cylindrical charge distribution surrounding a threading dislocation core that is shielded from the surrounding Schottky barrier potential, we can write the Coulombic potential of the charged dislocation according to[31]

$$\Phi_{\text{disl}} = \frac{1}{4}\frac{qN^+}{\varepsilon_s}r^2. \tag{14}$$

Here, Φ_{disl} is the magnitude of the Coulombic barrier, N^+ is the uniform ionized positive charge surrounding the negatively charged dislocation in the *n*-type GaN, and r is the cylindrical depletion radius that is assumed to be abrupt. This simple model does not implicitly consider the band bending due to the Schottky contact, and assumes all shallow dopants are ionized. However, there is ample evidence for the presence of significant amounts of additional space charge localized around dislocations due to deep levels that may be associated with point defects that segregate to dislocations or dislocations themselves.[32–34] Moreover, line charge densities in the range of 0.3–2.0 e/unit cell in the *c*-axis direction have been reported for GaN.[35–37] Hence, it is reasonable to expect the occurrence of local Fermi level pinning around dislocations. For the sake of calculation, if we estimate a moderate line charge density from previous reports of 1 e/unit cell in the *c* direction, this gives an estimated local defect density necessary to achieve charge balance of approximately 1.5×10^{16} cm^{-3} using the following equation:

$$\rho_l = \pi r^2 N^+, \tag{15}$$

where ρ_l is the line charge density per unit length. This value is consistent with the concentration of deep levels associated with dislocation-point defect complexes reported in earlier work,[32] noting that these calculations are not diluted by lower point defect concentrations in regions between dislocations. The magnitude of the calculated barrier associated with this amount of charge at each dislocation, estimated using Eq. (15), is ~0.2 V. This value is in reasonable agreement with earlier reports of local barriers surrounding dislocations in *n*-GaN having magnitudes of ~0.3 V, based on deep level transient spectroscopy (DLTS) pulse filling experiments,[32] and is also consistent with the earlier discussion regarding reduced local carrier conduction associated with dislocations having either pure edge or mixed character.

IV. CONCLUSION

The detailed *I-V* characteristics of Ni-*n*-GaN Schottky diodes were investigated as a function of threading dislocation density over a range of 3×10^7–7×10^8 cm^{-2}. Nearly identical barrier heights in the range of 1.11–1.13 eV were measured using *I-V-T* fitting. Independent internal photoemission measurements confirmed these values and their invariance with TDD over the range investigated here. The nearly constant barrier heights between the two sample types appeared, however, to be in contrast with the observed *I-V* characteristics that display an anomalous shift in the forward bias-turn-on voltage to higher values for higher TDD samples. Detailed calculations showed this shift to be related to differences in the extracted, apparent Richardson constant for which the higher TDD diodes display values significantly lower than the ideal value. A model is presented that accounts for this difference in terms of an equivalent circuit consisting of two parallel Schottky diodes, one representing an ideal *n*-GaN Schottky interface and the other representing regions where dislocations intersect the interface. The larger fraction of the interface that is influenced by dislocations for the higher TDD sample is shown in effect to reduce the area of ideal Ni–GaN contact, which is not accounted for in the usual extraction of the Richardson constant for which total device areas are used. By applying this simple model to the data, the difference in extracted Richardson constant values between the two sample types and the theoretical value is rectified, and it is shown that this completely accounts for the apparent shift in the forward bias *I-V* turn-on voltage. More detailed consideration of this model allows extraction of local barrier height increases in the vicinity of dislocations crossing the Schottky interface, the results of which are consistent with independent work reported previously for local charging effects.

ACKNOWLEDGMENTS

The work at OSU is supported by the Office of Naval Research (ONR) and the ONR-sponsored Center for Advanced Nitride Electronics (CANE) and Millimeter Wave Initiative for Nitride Electronics (MINE) MURIs (P. Maki and H. Dietrich). Also, the authors acknowledge K. Nakano and R. Fitch of the Wright Patterson Air Force Base for device processing.

[1] Y. Ohno and M. Kuzuhara, IEEE Trans. Electron Devices **48**, 517 (2001).
[2] M. Razeghi, Proc. IEEE **90**, 1006 (2002).
[3] H. Morkoc, A. Di Carlo, and R. Cingolani, Solid-State Electron. **46**, 157 (2002).
[4] W. Mönch, J. Vac. Sci. Technol. B **17**, 1867 (1999).
[5] A. C. Schmitz, A. T. Ping, M. A. Khan, Q. Chen, and J. W. Yang, Semicond. Sci. Technol. **11**, 1464 (1996).
[6] V. M. Bermudez, J. Appl. Phys. **86**, 1170 (1999).
[7] S. T. Bradley, S. H. Goss, J. Hwang, W. J. Schaff, and L. J. Brillson, Appl. Phys. Lett. **85**, 1368 (2004).
[8] Z. Z. Bandic, P. M. Bridger, E. C. Piquette, and T. C. McGill, Appl. Phys. Lett. **73**, 3276 (1998).
[9] A. Hierro, D. Kwon, S. A. Ringel, M. Hansen, J. S. Speck, U. K. Mishra, and S. P. DenBaars, Appl. Phys. Lett. **76**, 3064 (2000).
[10] S. M. Sze, *Physics of Semiconductor Devices* (Wiley, New York, 1981), pp. 256–289.
[11] A. M. Witowski, K. Pakuła, J. M. Baranowski, M. L. Sadowski, and P. Wyder, Appl. Phys. Lett. **75**, 4154 (1999).
[12] R. H. Fowler, Phys. Rev. **38**, 45 (1931).
[13] E. H. Rhoderick and R. H. Williams, *Metal-Semiconductor Contacts*, 2nd ed. (Oxford University, New York, 1988), pp. 111–113.
[14] N. Newman, M. van Schilfgaarde, T. Kendelwicz, M. D. Williams, and W. E. Spicer, Phys. Rev. B **33**, 1146 (1986).

[15]S. Karatas, S. Altindal, A. Türüt, and A. Özmen, Appl. Surf. Sci. **217**, 250 (2003).
[16]J. H. Werner and H. H. Güttler, J. Appl. Phys. **69**, 1522 (1990).
[17]P. Hacke, T. Detchprohm, K. Hiramatsu, and N. Sawaki, Appl. Phys. Lett. **63**, 2676 (1993).
[18]J. D. Guo, F. M. Pan, M. S. Feng, R. J. Guo, P. F. Chou, and C. Y. Chang, J. Appl. Phys. **80**, 1623 (1996).
[19]E. V. Kalinina, N. I. Kuznetsov, A. I. Babanin, V. A. Dmitriev, and A. V. Shchukarev, Diamond Relat. Mater. **6**, 1528 (1997).
[20]L. S. Yu, Q. Z. Liu, Q. J. Xing, D. J. Qiao, and S. S. Lau, J. Appl. Phys. **84**, 2099 (1998).
[21]T. Hashizume, J. Kotani, and H. Hasegawa, Appl. Phys. Lett. **84**, 4884 (2004).
[22]T. Sawada, Y. Ito, N. Kimura, K. Imai, K. Suzuki, and S. Sakai, Appl. Surf. Sci. **190**, 326 (2002).
[23]A. Barinov, L. Gregoratti, B. Kaulich, M. Kiskinova, and A. Rizzi, Appl. Phys. Lett. **79**, 2752 (2001).
[24]P. J. Hansen *et al.*, Appl. Phys. Lett. **72**, 2247 (1998).
[25]G. Koley and M. G. Spencer, Appl. Phys. Lett. **78**, 2873 (2001).
[26]O. Weidemann, E. Monroy, E. Hahn, M. Stutzmann, and M. Eickhoff, Appl. Phys. Lett. **86**, 083507 (2005).
[27]E. J. Miller, D. M. Schaadt, E. T. Yu, C. Poblenz, C. Elsass, and J. S. Speck, J. Appl. Phys. **91**, 9821 (2002).
[28]B. S. Simpkins, E. T. Yu, P. Waltereit, and J. S. Speck, J. Appl. Phys. **94**, 1448 (2003).
[29]B. Heying, R. Averbeck, L. F. Chen, E. Haus, H. Riechert, and J. S. Speck, J. Appl. Phys. **88**, 1855 (2000).
[30]L. Min *et al.*, Phys. Status Solidi C **1**, 2438 (2004).
[31]J.-L. Farvacque, Z. Bougrioua, and I. Moerman, Phys. Rev. B **63**, 115202 (2001).
[32]A. Hierro, A. R. Arehart, B. Heying, M. Hansen, J. S. Speck, U. K. Mishra, S. P. DenBaars, and S. A. Ringel, Phys. Status Solidi B **228**, 309 (2001).
[33]A. Hierro, M. Hansen, L. Zhao, J. S. Speck, U. K. Mishra, S. P. DenBaars, and S. A. Ringel, Phys. Status Solidi B **228**, 937 (2001).
[34]Z.-Q. Fang, D. C. Look, and L. Polenta, J. Phys.: Condens. Matter **14**, 13061 (2002).
[35]J. Cai and F. A. Ponce, Phys. Status Solidi A **192**, 407 (2002).
[36]C. Jiao and D. Cherns, J. Electron Microsc. **51**, 105 (2002).
[37]D. Cherns, C. G. Jiao, H. Mokhtari, J. Cai, and F. A. Ponce, Phys. Status Solidi B **234**, 924 (2002).